

Trapped-ion decay spectroscopy towards the determination of ground-state components of double-beta decay matrix elements

T. Brunner^{1,2a}, A. Lapierre^{1b}, C. Andreoiu³, M. Brodeur⁴, P. Delheji¹, S. Ettenauer^{1,5c}, D. Frekers⁶, A.T. Gallant^{1,5}, R. Gernhäuser², A. Grossheim¹, R. Krücken^{2d}, A. Lennarz^{1,6}, D. Lunney⁷, D. Mücher², R. Ringle^{1e}, M.C. Simon^{1f}, V.V. Simon^{1,8,9g}, S.K.L. Sjøe^{1h}, K. Zuber¹⁰, and J. Dilling^{1,5}

¹ TRIUMF, Vancouver, BC, V6T 2A3, Canada

² Physik Department E12, Technische Universität München, D-85748 Garching, Germany

³ Department of Chemistry, Simon Fraser University, Burnaby, BC, V5A 1S6, Canada

⁴ Department of Physics, University of Notre Dame, Notre Dame, IN, 46556 US

⁵ Department of Physics and Astronomy, University of British Columbia, Vancouver, BC, V6T 1Z1, Canada

⁶ Westfälische Wilhelms-Universität Münster, D-48149 Münster, Germany

⁷ CSNSM-IN2P3-CNRS, Université de Paris Sud, 91405 Orsay, France

⁸ Fakultät für Physik und Astronomie, Ruprecht-Karls-Universität Heidelberg, D-69120 Heidelberg, Germany

⁹ Max-Planck-Institut für Kernphysik, D-69117 Heidelberg, Germany

¹⁰ Institut für Kern- und Teilchenphysik, Technische Universität Dresden, D-01069 Dresden, Germany

the date of receipt and acceptance should be inserted later

Abstract A new technique has been developed at TRIUMF's TITAN facility to perform in-trap decay spectroscopy. The aim of this technique is to eventually measure weak electron capture branching ratios (ECBRs) and by this to consequently determine GT matrix elements of $\beta\beta$ decaying nuclei. These branching ratios provide important input to the theoretical description of these decays. The feasibility and power of the technique is demonstrated by measuring the ECBR of ^{124}Cs .

Key words. Nuclear matrix element, neutrinoless double-beta decay, Penning trap, in-trap decay spectroscopy

PACS. 37.10.Ty – 29.30.Kv – 23.40.-s – 14.60.Lm – 14.60.St

1 The $\beta\beta$ decay matrix element

Measuring the neutrino properties poses great challenges in modern physics. Despite numerous efforts, the character of the neutrino still remains a mystery, i.e., whether it is a Dirac or Majorana particle [1, 2]. A powerful approach to shed light on this question is through $\beta\beta$ -decay

^a *Present address:* Stanford University, Stanford, CA, 94305, USA e-mail: tbrunner@stanford.edu

^b *Present address:* NSCL, Michigan State University, East Lansing, MI, 48824, USA

^c *Present address:* Department of Physics, Harvard University, Cambridge, Massachusetts 02138, USA

^d *Present address:* TRIUMF, Vancouver, BC, V6T 2A3, Canada

^e *Present address:* NSCL, Michigan State University, East Lansing, MI, 48824, USA

^f *Present address:* Stefan Meyer Institute for subatomic Physics, Vienna, Austria

^g *Present address:* Helmholtz Institute Mainz, Germany

^h *Present address:* Los Alamos National Laboratory, Los Alamos, NM, 87544, USA

experiments [3–5]. Double-beta decay is a rare, second-order weak process, which is expected to happen in at least two modes, the zero-neutrino ($0\nu\beta\beta$) and the two-neutrino ($2\nu\beta\beta$) mode. The $2\nu\beta\beta$ decay has been observed in various isotopes with half-lives greater than 10^{18} years [6]. The $0\nu\beta\beta$ mode is forbidden in the Standard Model of particle physics as it violates lepton-number conservation. Moreover, the existence of the neutrinoless mode uniquely establishes the Majorana character of the neutrino [7, 8], and if the mass term is the leading contribution, one can deduce the effective Majorana neutrino mass $\langle m_\nu \rangle$ from the half-life of the decay:

$$\left(T_{1/2}^{0\nu}\right)^{-1} = G^{0\nu}(Q, Z) |M^{0\nu}|^2 \langle m_\nu \rangle^2. \quad (1)$$

Here, $G^{0\nu}(Q, Z)$ is the phase-space factor and $M^{0\nu}$ is the nuclear matrix element (NME). Currently, several models provide values for $M^{0\nu}$ (see for example [1, 9–15]). In order to extract a value of m_ν , $M^{0\nu}$ must be known with reasonable precision. Frequently, theoretical approaches use the $2\nu\beta\beta$ decay to test their models (see for example [16]). Recent experiments have shown that the 2ν

NME is rather sensitive to the ground-state properties of the nuclear wave function [17–20]. An experimental access to probe these ground-state nuclear wave functions and thus part of the Gamow-Teller matrix element is through spectroscopic measurements (see Ref. [21] and references therein). They can be obtained from measurements of the branching ratios of the intermediate nucleus, i.e., the electron capture (EC) and β branching ratios (BRs) of the ground-state decay of the intermediate nucleus. For all intermediate nuclei in $\beta\beta$ decays the ECBRs are small and the EC signature is the emission of X-rays by the daughter atom. This poses a formidable experimental challenge for ECBR measurements. In addition, the short-lived intermediate nucleus has to be produced at a radioactive isotope facility, which almost always delivers isobaric contamination.

In previous ECBR measurements such as the one of ^{100}Tc , the ECBR has been measured by the implantation of radioactive ^{100}Tc onto a tape [22]. This tape was then moved in front of several X-ray and β -particle detectors. The difficulties of this method arise from contaminations in the sample, the β -particle background from dominating β branches, and possible X-ray attenuation in the implantation material. Improvements of this measurement were accomplished by applying the technique of trap-assisted decay spectroscopy at Jyväskylä [23]. Here, the sample was isobarically purified in a Penning trap by means of a mass-selective buffer-gas cooling technique [24]. The purified sample was then implanted onto an Al foil in front of a X-ray detector. The Al foil was embedded into a plastic scintillator used to veto β particles. This technique improved the uncertainty of the previous ECBR measurement of ^{100}Tc by a factor of two [23]. However, it still suffers from a large background due to secondary radiation and X-ray attenuation by the implantation material. In order to overcome these drawbacks a novel technique has been proposed [21] and developed at TITAN using an open-access Penning trap to perform in-trap decay spectroscopy. In this scheme the strong magnetic field of the trap guides β particles away from the X-ray detectors and thereby reduces their contribution to the X-ray spectrum. Furthermore, established ion-trap techniques available at TITAN allow for isobaric purification of the sample in the future. Ion traps are nowadays well established tools for precision experiments at radioactive beam facilities [25], however, this in-trap application is unique to the TITAN set-up. In this paper the feasibility of this technique is demonstrated by measuring the ECBR of ^{124}Cs .

2 TITAN-EC Setup

TITAN [26, 27] is TRIUMF’s Ion Trap facility for Atomic and Nuclear science which currently consists of the Radio-Frequency Quadrupole (RFQ) [28, 29], the Electron Beam Ion Trap (EBIT) [30, 31] and the mass Measurement Penning Trap (MPET) [32]. An engineering model of the experimental setup is given in Fig. 1.

For this ECBR measurement at TITAN, the EBIT is operated as a spectroscopy-Penning trap without the

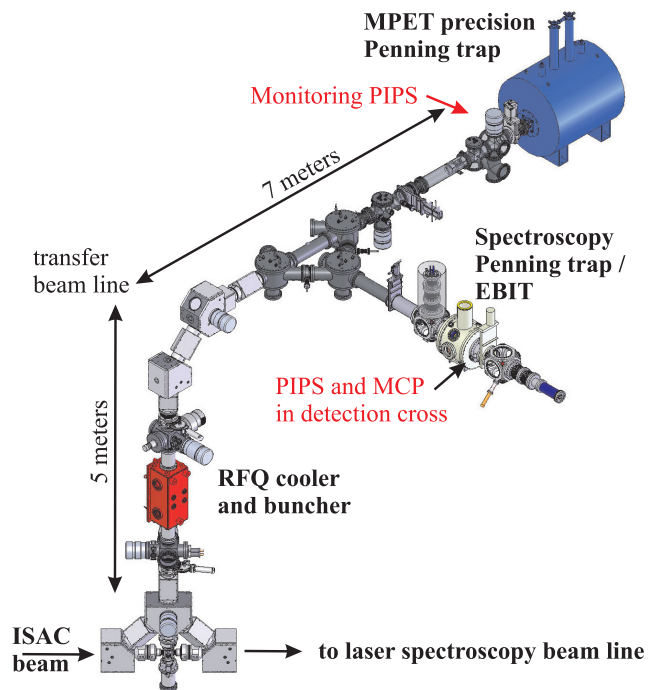


Figure 1. (color online) Engineering rendering of the TITAN facility showing RFQ, MPET, EBIT as well as the positions of the PIPS detectors.

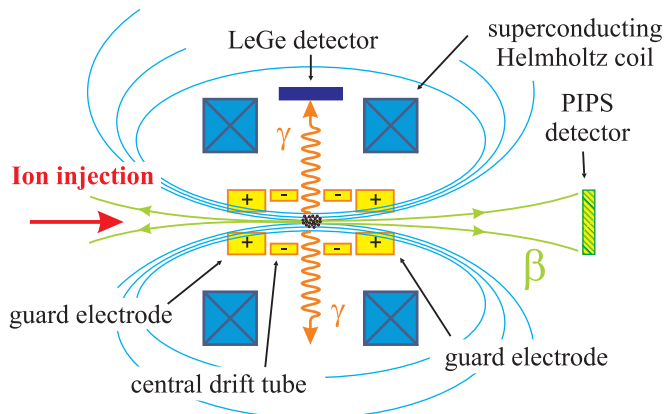


Figure 2. (color online) Schematic illustration of the in-trap decay spectroscopy Penning trap at TITAN. After injection, radioactive ions are trapped for up to 50 ms. While stored inside the trap, their electron-capture decays are monitored by a LeGe detector installed on a radial view port perpendicular to the ion beam line. Electrons resulting from β decays are guided out of the trap-center region towards both ends by the trap’s strong magnetic field. Beta particles are detected with a PIPS detector at one end.

electron beam. During in-trap decay spectroscopy measurements radioactive ions are stored at the center of the trap. Gamma- and X-rays following an EC event are emitted isotropically, while β particles are guided out of the trap along the axis of the magnetic field (up to 5 T in the present experiment, see Fig. 2). These β particles are detected by a Passivated Implanted Planar Silicon (PIPS)

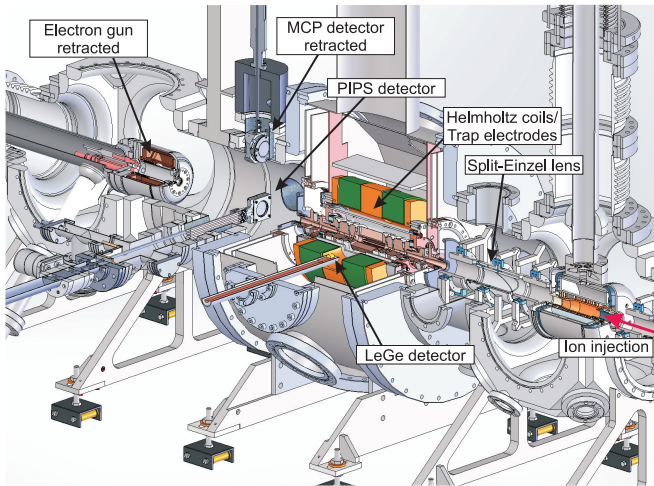


Figure 3. (color-online) Schematic rendering of the setup illustrating the trap center geometry as well as the position of LeGe detector (yellow cylinder), PIPS detector and retracted electron gun and MCP.

detector placed at one side of the trap [33] labeled PIPS in Fig. 1 and Fig. 2. The radial confinement provided by the magnetic field prevents electrons from reaching the X-ray detector. This spatial separation between X-ray and β -particle detection constitutes the significant advantage of this technique compared to conventional ones. A schematic illustration of the setup of the spectroscopy trap is presented in Fig. 2.

The radially confining magnetic field of the trap is generated by a pair of superconducting coils arranged in a Helmholtz-like configuration [31]. This configuration allows for visible access to trapped ions owing to radial openings in the magnet assembly and the central trap electrode. This electrode is eight-fold segmented with slit apertures between each segment. In total, seven of these view ports towards the trap center are available for in-trap decay spectroscopy [31]. The measurements presented here were obtained with only one low-energy planar Ge detector (LeGe, Canberra model GUL 0110P, $\phi 11.3$ mm, 10 mm thick) used for γ - and X-ray detection. It was installed inside the vacuum vessel and positioned between the coils at a distance of ~ 10 cm from the trap center.

3 In-Trap Decay Spectroscopy

The feasibility of measuring electron-capture branching ratios with a Penning trap has been demonstrated by measuring the ECBR of ^{124}Cs within this work. This isotope was chosen due to its relatively large EC branch of 10.0(7)%. During this measurement in-trap decay spectroscopy of ^{126}Cs has been performed as well. Cesium-126 has been used to calibrate the efficiency of the detector. Both isotopes were produced as singly charged ions at the TRIUMF ISOL-type facility ISAC [34] by bombarding a tantalum target with a $50 \mu\text{A}$ proton beam at 500 MeV delivered by the TRIUMF cyclotron. Radioactive cesium atoms were surface-ionized and then passed

through a high-resolution dipole magnet (resolving power $R \sim 3000$) to reduce isobaric contamination. Production yields were $1.3 \cdot 10^7/\text{s}$ for ^{124}Cs , $2.5 \cdot 10^5/\text{s}$ for $^{124\text{m}}\text{Cs}$, and $1.6 \cdot 10^7/\text{s}$ for ^{126}Cs measured at the ISAC-I yield station [35]. At TITAN, the radioactive ions were cooled and bunched by the RFQ [28, 29]. To identify the dominating isotope in the beam and to estimate the ion bunch intensity, 10 bunches were extracted from the RFQ at a rate of 10 Hz and transported to a surface-barrier detector assembly in front of the MPET. This detector assembly consisted of an Al foil in front of a Passivated Implanted Planar Surface-barrier detector (Canberra PIPS detector [36]). The ions were implanted onto the Al foil. This detector is indicated as monitoring PIPS in Fig. 1. The isotopes ^{124}Cs and ^{126}Cs were identified by their half-lives. The half life of ^{124}Cs was determined as 30.9(1)s which is in agreement with the literature value of 30.8(5) s [37], however with a slightly improved uncertainty. Assuming a β -detection efficiency of $(25 \pm 10)\%$ ion bunch intensities at 10 Hz were estimated, with exponential fits to their decay times, to be $(2.8 \pm 1.1) \cdot 10^5$ ions/bunch for ^{124}Cs and $(4.4 \pm 2.1) \cdot 10^5$ ions/bunch for ^{126}Cs . The efficiency is the product of intrinsic efficiency and geometric acceptance of the detector. The latter is the main contributor to the uncertainty of the total efficiency due to the uncertainty of the distance of (6 ± 1) mm between detector and Al foil. The intrinsic detection efficiency was calculated by integrating the β spectrum [38]. Based on this, an intrinsic detection efficiency of $\sim 99\%$ was determined assuming that electrons below 250 keV were stopped by the $20 \mu\text{m}$ thick Al foil and the detector's dead layer, and thus not detected. The decay rate spectra were analyzed in order to investigate the possibility of isobaric Ba contamination. No significant contribution was found.

3.1 Measurement Cycle and Data Acquisition

During an ECR measurement radioactive ions lost inside the RFQ and along the TITAN beam lines contribute to the photon background [39]. In order to correct the in-trap decay spectrum for this background in-trap decay and background spectra were recorded successively. During the measurement period Δt_{meas} , γ - and X-rays following radioactive decays were detected with the LeGe detector. After this measurement, the trap was emptied by extracting the remaining ions. About 1 ms after each ion bunch was extracted from the trap, a background measurement was started for Δt_{BGND} . Typically, storage and background-measurement time intervals of $\Delta t_{meas} = \Delta t_{BGND} = 25$ ms were used. A cycle with $\Delta t_{meas} = \Delta t_{BGND} = 50$ ms was also applied for a measurement period of one hour during the measurement of the calibrant ^{126}Cs .

The energy of the γ - and X-rays deposited in the crystal of the low-energy Ge detector was amplified by a transistor-reset amplifier. This amplifier provided an output voltage signal with a rising edge between 0 and 5 V, which was proportional to the deposited energy. The amplifier also provided a transistor-reset signal, which was used to

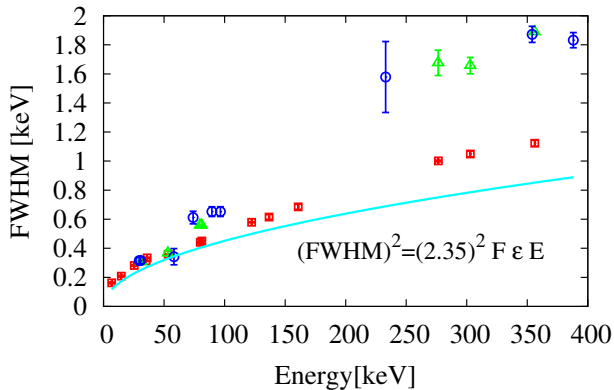


Figure 4. (color online) Energy resolution (FWHM) of the LeGe detector in a zero (\square) and 2 T magnetic field environment. The zero-field FWHM was measured using ^{57}Co and ^{133}Ba sources. The resolution at 2 T was determined using ^{133}Ba (\circ) as well as ^{124}Cs and ^{126}Cs calibrations lines (\triangle). The solid line represents the resolution limit of a Ge detector determined by the Fano factor, F , and the energy, ε , required to create an electron-hole pair [40].

disable the data acquisition while the voltage signal was reset to its initial value. Both the energy and transistor-reset signals were split and fed into two ORTEC DSPEC units, called 319 and 321. These two units were then gated to record data during the time intervals Δt_{meas} (DSPEC 321) or Δt_{BGND} (DSPEC 319).

After the ions were extracted from the trap back into the beam line they were sent to the monitoring PIPS detector installed in front of the MPET [36] (see Fig. 1). The β -particle counting rate of this detector was then used to continuously monitor the intensity stability of the experiment [39].

3.2 Influence of the Magnetic Field on the LeGe Detector

The LeGe detector, which is installed on one of the EBIT's radial ports, was inserted between the two Helmholtz coils at a position close to the trap center. During the experiment the magnetic field at the trap center was 5 T resulting in a calculated residual field at the position of the LeGe detector of about 2 T with its orientation parallel to the surface of the crystal. It was observed that this magnetic field strength broadens the photopeaks. Figure 4 shows the full width at half maximum (FWHM) of photopeaks recorded with the LeGe detector in a no-field and 2 T field environment, respectively. No-field (0 T) refers to a residual field dominated by the earth's magnetic field. No change of detection efficiency was observed within the uncertainty. This experimental finding necessitates further investigations.

3.3 Spectroscopic Measurements

The summed decay spectrum of the ^{124}Cs EC-process is presented in Fig. 5. The red spectrum was recorded while ions were stored in the ion trap and the black spectrum shows the background spectrum obtained after each ion bunch was extracted from the trap. Indicated in these spectra are the most prominent photopeaks and their origins. Clearly present are signatures of the isomer ^{124m}Cs , i.e., the Cs K -shell X-ray lines of the electron conversion process and the photopeak at 211.6 keV from the depopulation of the 3^+ level in ^{124m}Cs . Also present in the spectrum are the Pb X-ray lines which appear in both background and in-trap decay spectra. It cannot be excluded that solder containing Pb was used to contact the Ge crystal, where Pb acts as an X-ray radiator. The Pb photopeaks do not overlap with any of the X-ray peaks of interest. In the in-trap decay spectrum a shoulder is observed between 250 keV and 350 keV. This shoulder occurs in the ^{124}Cs and ^{126}Cs spectra. Calibration spectra with ^{133}Ba show that the efficiency with which both DSPEC units record events degrades at energies above ~ 120 keV. In particular, a drop in efficiency is observed at 250 keV for DSPEC 321 (background DSPEC) and 300 keV for DSPEC 319 (in-trap measurement DSPEC). This artifact does, however, not affect the analysis of the data presented in this publication.

A focused view of the X-ray region is presented in Fig. 6 showing the advantage of the new in-trap decay spectroscopy technique. The dominating β decay did not contribute significant background to the X-ray spectrum. Positrons reaching the LeGe detector would have resulted in a drastically increased background in the in-trap decay spectrum (solid, red line). When ions are stored in the trap a clear xenon K -shell X-ray signature is visible originating from electron-capture decays of ^{124}Cs . Also present are the cesium K -shell X-ray lines that originate from the de-excitation of ^{124m}Cs . Note that no K -shell X-ray peaks are observed in the background spectrum (dashed, black line). Comparing these two spectra one can conclude that no significant ion losses occurred radially and within the line of sight of the detector.

The clear distinction between in-trap decay and background spectra worsens in the higher energy range. This is evident in the 211.6 keV photopeak of the isomeric state and the 354 keV photopeak originating from the 2^+ level in ^{124}Xe . The latter peak is presented in Fig. 7 with solid, red and dashed, black line being the in-trap decay and background spectra, respectively. In this figure the photopeak is present in both spectra. In the background spectrum it originates from ^{124}Cs ions that were lost along the beam line during injection and ejection as well inside the RFQ. The material surrounding the LeGe detector does not provide sufficient shielding. This agrees with previous observations where ^{126}Cs was deposited in the RFQ and the 354 keV peak was present in the LeGe detector spectrum [39]. It is therefore essential to measure both in-trap decay and background spectra immediately after each other.

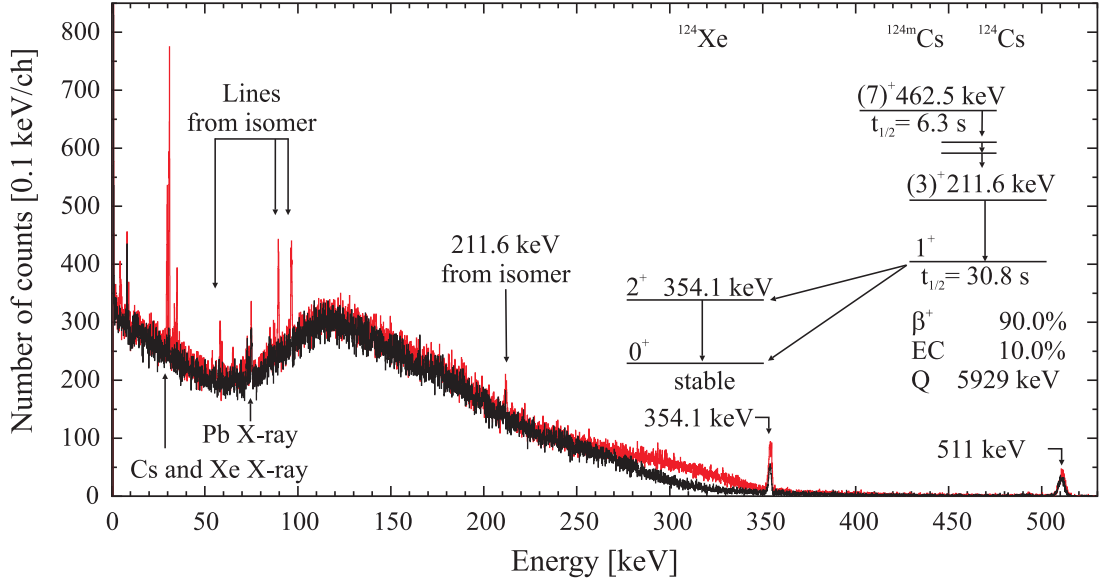


Figure 5. (color online) Summed spectrum of the decay of ^{124}Cs . The red spectrum was recorded with ^{124}Cs stored in the trap whereas the black spectrum represents the background which was recorded with no ions stored. The measurement times of both spectra were identical. The simplified level scheme indicates the origin of the dominant photopeaks (from [37], ECBR calculated with [41]).

The ^{126}Cs spectra that are used for calibration are presented in Fig. 8 and Fig. 9 for X-ray and γ region, respectively. During this measurement ions were lost inside the trap center and contributed to the X-ray background spectrum presented in Fig. 8. The 388 keV photopeak also has a stronger contribution in the background spectrum as compared to the 354 keV photopeak of ^{124}Cs shown in Fig. 7. Ion beam intensity as well as injection parameters were different for ^{124}Cs and ^{126}Cs . These effects need to be investigated in future developments of this technique in order to improve the signal-to-background ratio.

3.4 Data Analysis

The electron capture branching ratio is defined as the number of decays by electron captures N_{EC} divided by the total number of decays N . The quantity accessible in our experiment is the number of detected K -shell X-rays emitted following an electron capture defined as D_K^{meas} . The total number of decays N is extracted from the photopeak counts D_γ^{meas} of the lowest 2^+ state of the daughter nucleus of the β branch. The photopeak intensity I_γ was taken from literature [37] and the ECBR can then be written as

$$BR(EC) = \frac{1}{\omega_K \cdot f_K} \left(\frac{\varepsilon_{int}^{det}(E_\gamma) I_\gamma D_K^{meas}}{\varepsilon_{int}^{det}(E_K) D_\gamma^{meas}} - \omega_K I_K^{CE} \right), \quad (2)$$

with I_K^{CE} being the total intensity of the K -shell conversion electrons, ω_K being the fluorescence yield, and f_K the probability that an EC event creates a vacancy in the K -shell. Since both, X-ray and γ photons are recorded with the same detector the geometrical acceptance cancels out.

The detection efficiency $\varepsilon_{int}^{det}(E)$ describes the intrinsic detection efficiency at X-ray and γ energies E_K and E_γ , respectively. The latter equation simplifies to

$$BR(EC) = \frac{I_K - I_{CE}}{\omega_K \cdot f_K}, \quad (3)$$

using the total K -shell intensity

$$I_K = \frac{\varepsilon_{int}^{det}(E_\gamma) I_\gamma D_K^{meas}}{\varepsilon_{int}^{det}(E_K) D_\gamma^{meas}}, \quad (4)$$

and subtracting the K -shell X-ray intensity due to conversion electrons $I_{CE} = \omega_K I_K^{CE} = 0.888(5)[42] \cdot 0.010285(113)[37] = 0.00913(11)$. The detector efficiency term in the X-ray energy region cancels out if another isotope of the same element with a well-known X-ray intensity is measured under the same experimental conditions. This known X-ray intensity can be expressed as

$$I_{K'} = \frac{D_{K'}^{meas} I_{\gamma'} \varepsilon_{int}^{det}(E_{\gamma'})}{D_{\gamma'}^{meas} \varepsilon_{int}^{det}(E_{K'})}. \quad (5)$$

One can re-write Eq. 4 as

$$I_K = I_{K'} \frac{D_K^{meas} D_{\gamma'}^{meas} I_\gamma \varepsilon_{int}^{det}(E_\gamma)}{D_{K'}^{meas} D_\gamma^{meas} I_{\gamma'} \varepsilon_{int}^{det}(E_{\gamma'})}, \quad (6)$$

if the X-ray energies are identical, as for isotopes of the same element. Therefore, only the ratio $\varepsilon_{int}^{det}(E_\gamma)/\varepsilon_{int}^{det}(E_{\gamma'})$ needs to be known. For photon energies above ~ 120 keV the detector response is well known and the self-shielding of the calibration sources is less of a concern than in the X-ray region. Typically, E_γ and $E_{\gamma'}$ are above 120 keV. The ECBR of ^{124}Cs was determined by applying the described method using ^{126}Cs for calibration.

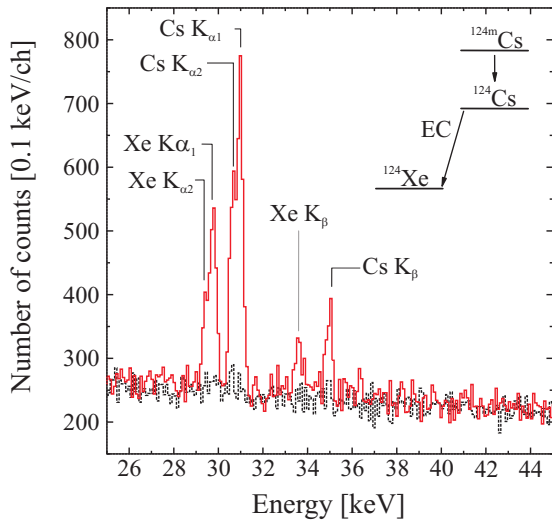


Figure 6. (color online) Energy region showing X-ray lines resulting from the decay of ^{124}Cs . Dashed, black and solid, red spectrum were recorded during Δt_{BGND} and Δt_{meas} , respectively. The measurement time was 6 h.

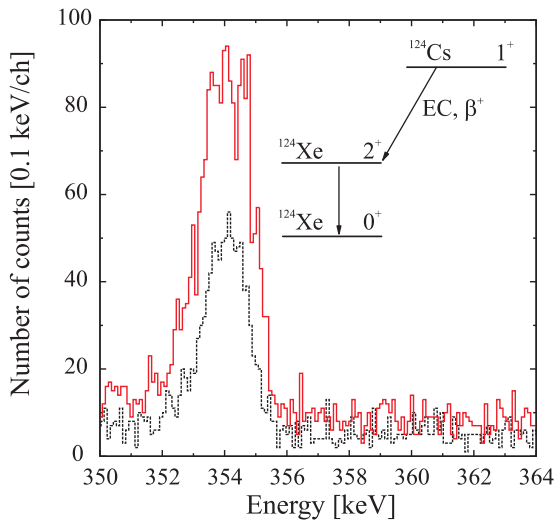


Figure 7. (color online) 354 keV photopeak originating from the 2^+ level of ^{124}Xe . Dashed, black and solid, red spectrum were recorded during Δt_{BGND} and Δt_{meas} , respectively. The spectrum is the sum of 6 h of measurement.

3.5 Results

The photopeak counts D_K^{meas} and D_γ^{meas} of the ^{124}Cs , ^{126}Cs and calibration spectra have been determined by the method of maximum likelihood. In the fit of X-ray spectra the relative K -shell intensities and energies were constrained to their known values [43].

The measurement periods $\Delta t_{meas} = \Delta t_{BGND}$ of 25 ms and 50 ms were short compared to the half-lives of 30.8(5) s and 1.64(2) min for ^{124}Cs and ^{126}Cs , respectively. Therefore, the decay rate was considered constant throughout both measurement periods. This assumption is valid to a level of the order of 10^{-4} . Based on this assumption, the peak intensity of the background measurement recorded

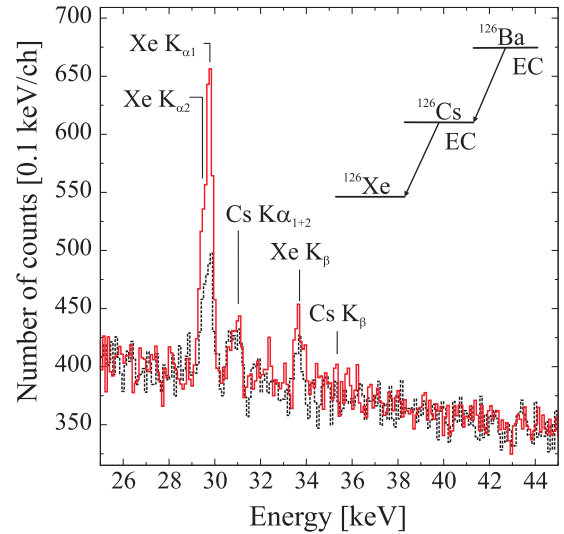


Figure 8. (color online) Energy region showing X-ray lines resulting from the decay of ^{126}Cs . Dashed, black and solid, red spectrum were recorded during Δt_{BGND} and Δt_{meas} , respectively. The spectra is the sum of 12 h of measurement time.

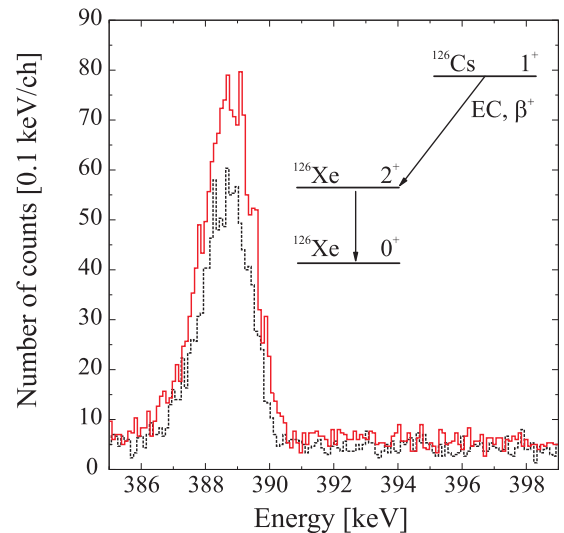


Figure 9. (color online) 388 keV photopeak originating from the 2^+ level of ^{126}Xe . Dashed, black and solid, red spectrum were recorded during Δt_{BGND} and Δt_{meas} , respectively. The total measurement time was 12 h.

during Δt_{BGND} was subtracted from the peak intensity measured during Δt_{meas} . The measurement was divided into time slices. Within each time slice all settings were kept constant. Cesium-126 was measured in five time slices for a total of 12 hours while ^{124}Cs was measured in two time slices for a total of 6 hours. The resulting ^{124}Cs and ^{126}Cs photopeak intensities are presented in Table 1 and Table 2, respectively. After the experiment was performed it was discovered that the DSPEC units truncate the energy signal, i.e., the number of recorded counts in the spectrum does not correspond to the number of expected counts. Comparison with Monte-Carlo simulations shows that both DSPEC units attenuated energy

Table 1. Counts in the photopeaks of ^{124}Cs . The uncertainty is determined by the fit and listed in brackets. 0(10) is unphysical but arises from the fitting routine. For consistency reasons the value is presented this way. Two time slices (TS) of 4 and 2 hours were measured. The spectra within each time slice were summed prior to the analysis. The fourth column lists the γ -peak counts corrected for the different DSPEC inefficiencies. The last column indicates whether the data was recorded during Δt_{BGND} (BGND) or Δt_{meas} (storage).

TS [h]	X-ray peak Xe K_α & K_β	γ peak 354.1 keV	corr. γ peak 354.1 keV	
4	94(43)	549(28)	837(158)	BGND storage
	1074(66)	1152(40)		
2	0(10)	285(19)	434(84)	BGND storage
	490(42)	534(27)		

Table 2. Counts in the photopeaks of ^{126}Cs . The values are listed in the same way as those of ^{124}Cs presented in Table 1.

TS [h]	X-ray peak Xe K_α & K_β	γ peak 388 keV	corr. γ peak 354.1 keV	
3	399.67(67)	704(31)	843(125)	BGND storage
	1218.91(69)	1038(42)		
1	164(45)	382(22)	271(43)	BGND storage
	591(53)	479(26)		
2	494.89(62)	730(30)	874(128)	BGND storage
	864.67(68)	896(34)		
3	513.75(62)	667(29)	798(118)	BGND storage
	1055.45(74)	947(35)		
3	480.26(58)	603(27)	722(107)	BGND storage
	963.81(68)	799(32)		

signals of photon energies above ~ 120 keV. At photopeak energies of ~ 300 keV this truncation amounts to more than two orders of magnitude. During the experiment ^{133}Ba calibration spectra were recorded to identify possible drifts in the data acquisition. However, the number of counts in these spectra are low hence it is difficult to use them for calibration. The ratio of photopeak counts recorded with DSPECs 319 and 321 was calculated for all peaks in the ^{133}Ba spectrum. The ratio in the X-ray region agrees with unity within uncertainty. However, the ratio at photopeak energies 276.3 keV, 302.9 keV, and 356.0 keV is energy dependent following a linear curve. This curve determines how efficient DSPEC 319 records photons at the energies of 354 keV (^{124}Cs) and 388 keV (^{126}Cs) with respect to DSPEC 321. The extrapolated ratio was then used to correct the photopeaks recorded with DSPEC 321 at 354 keV and 388 keV. The corrected values as well as all extracted photopeak counts are listed in Table 1 and Table 2 for ^{124}Cs and ^{126}Cs , respectively. The corrected counts in the background spectrum were then subtracted from the counts of the spectroscopy spectrum and the ratios of $D_K^{meas}/D_\gamma^{meas}$ and $D_{K'}^{meas}/D_\gamma^{meas}$ were determined. These ratios were calculated independently for each time slice. The weighted average of this ratio was

then calculated for each isotope. The ratio $\frac{\varepsilon_{int}^{det}(E_\gamma)}{\varepsilon_{int}^{det}(E_{\gamma'})}$ was determined with the ^{133}Ba calibration spectrum recorded with DSPEC 319. The ^{133}Ba photopeaks at energies of 276.3 keV, 302.9 keV and 356.0 keV [44] were used to extract the ratio of efficiencies at 354 keV and 388 keV.

The ECBR of ^{124}Cs was calculated according to Eq. 3 and Eq. 6 to be $(22.7 \pm 8.9(\text{stat.}) \pm 14.8(\text{syst.}))\%$ and is based on the measured ratios $\frac{D_K^{meas}}{D_\gamma^{meas}}$ (^{124}Cs), $\frac{D_{K'}^{meas}}{D_\gamma^{meas}}$ (^{126}Cs), and $\frac{\varepsilon_{int}^{det}(E_\gamma)}{\varepsilon_{int}^{det}(E_{\gamma'})}$, $f_K = 0.841(60)$ [37], $\omega_K = 0.888(5)$ [42], $I_{CE} = 0.009133(113)$, and $I_{K'} = 0.146(2)$ [45]. Our value agrees with the literature value of 10.0(7)% [37, 41]. However, the truncated detection efficiency of the DSPEC units reduced the counts in the γ photopeak that was used for normalization. The inefficiency in detection of these photons artificially increases the ECBR and is accounted for in the large systematic uncertainty. This systematic uncertainty arises from the different efficiencies of DSPEC 319 and 321. Nevertheless, the presented measurement proves that these decay-spectroscopy experiments are feasible.

The use of detected β particles at the PIPS detector mounted at one side of the trap for normalization has been investigated. In detailed SIMION [46] simulations it was found that the number of electrons or positrons reaching the PIPS detector strongly depends on various parameters [33, 39]. Among those, the position of the decaying ions (i.e. the ion cloud size and density distribution inside the trap) has the largest impact. The probability of a β particle reaching the PIPS detector also depends on the Q value of the decay. Since the trap is cryogenic it is almost impossible to place a calibration source inside the trap center and map the β detection efficiency for various source locations. Hence the concept of using β particles for normalization purposes has been discarded.

The X-ray photopeak areas of ^{124}Cs and ^{126}Cs , and the 89.5 keV and 96.6 keV lines of ^{124m}Cs were used to estimate the number of ions that were injected into the trap. Only decays of stored ions were considered, i.e., the peak area recorded during the background measurement was subtracted from the decay measurement. The detection efficiency was extracted from PENELOPE simulations of the experimental setup. The extracted intensities are presented in Table 3. The intensities of ^{126}Cs were extracted for each time slice separately throughout the experiment. They varied over time due to slight changes in beam tune and delivered isotope intensity. The RFQ cycle that was applied during these measurements differs from the 10 Hz rate presented in Section 3. Furthermore, before being captured in the Penning trap the ion bunches had to pass two additional electrostatic 45° bender where ions could have been lost. This could explain the lower ion bunch intensities listed in Table 3 compared to the PIPS measurement presented earlier.

Table 3. Ion bunch intensities derived from the measured $^{124\text{g,m},126}\text{Cs}$ photopeak intensities and the duration of each time slice (TS). The value marked with \dagger was measured with $\Delta t_{\text{meas}} = \Delta t_{\text{BGND}} = 50$ ms. All other measurements were performed with 25 ms.

Isotope	TS	TS [h]	Ion bunch intensity
$^{124\text{m}}\text{Cs}$		6	$4.48(63) \cdot 10^3$
$^{124\text{g}}\text{Cs}$			$1.34(13) \cdot 10^5$
^{126}Cs	1	3	$2.65(32) \cdot 10^5 \dagger$
^{126}Cs	2	1	$2.54(54) \cdot 10^5$
^{126}Cs	3	2	$1.85(46) \cdot 10^5$
^{126}Cs	4	3	$1.80(32) \cdot 10^5$
^{126}Cs	5	3	$1.61(30) \cdot 10^5$

4 Future ECBR measurement

After the ECBR measurement described in this work the detection setup has been upgraded. The single LeGe detector has been replaced by seven custom-made lithium-drifted Silicon (Si(Li)) detectors installed at all available view ports of the trap. This increases the geometrical acceptance from $\sim 0.1\%$ [47] to $\sim 2.1\%$. The detectors are placed outside the vacuum vessel behind thin Be windows. This increased distance to the trap center reduces the magnetic field at the position of the crystal to less than 1 T. To further enhance the sensitivity of the setup towards smaller ECBRs passive low-activity Copper-Lead sandwich shields have been added to the Si(Li) detectors. Moreover, the addition of BGO crystals as active Compton-suppression shielding has been studied, and a prototype is being constructed. The data acquisition system has been upgraded by replacing the DSPECs with sampling analog-to-digital converters (Struck SIS3302) [48], effectively eliminating any rate or energy dependent biases. These upgrades significantly reduce the background while increasing acceptance and mitigate the presented issues with the DSPEC DAQ.

5 Conclusion

A new technique has been developed at the TITAN facility to measure the ground-state transition strength of intermediate nuclei in $\beta\beta$ decays utilizing an open-access Penning trap. The feasibility and power of this in-trap decay spectroscopy technique have been demonstrated and various systematic studies have been performed. Within these studies an electron-capture decay of ions stored in a Penning trap has been observed for the first time [47, 49]. During the ECBR measurement of ^{124}Cs it was observed that ion losses along the beam line also contribute to the recorded photon spectrum, dominantly for photopeak energies above ~ 120 keV. A measurement cycle has been developed and applied to record background spectra immediately after the ions were extracted from the trap. With this technique and the upgraded experimental setup the determination of ECBRs as low as 10^{-5} is within reach.

6 Acknowledgment

TRIUMF receives federal funding via a contribution agreement with the National Research Council of Canada (NRC). This work was partly funded by NSERC and by the Deutsche Forschungsgemeinschaft (DFG) under grant FR 601/3-1. T.B. acknowledges support by evangelisches Studienwerk e.V. Villigst, A.G. acknowledges support from NSERC PGS-M program, V.V.S from the Studienstiftung des Deutschen Volkes and S.E. from the Vanier CGS program. We acknowledge the great support of TRIUMF and ISAC operations. We thank I. Ostrovskiy for fruitful discussions on data analysis and statistics. Also thanked are C. Pearson, S. Williams, S. Daviel, and P.-A. Amaudruz for their help with the DAQ system. We would especially like to thank TITAN's technologist M. Good for his help in setting up this experiment.

References

1. W. C. Haxton, G. J. Stephenson, *Progress in Particle and Nuclear Physics* **12**, 409 (1984)
2. M. Doi, T. Kotani, E. Takasugi, *Progress of Theoretical Physics Supplement* **83**, 1 (1985)
3. H. Ejiri, *Journal of the Physical Society of Japan* **74**, 8, 2101 (2005)
4. F. T. Avignone, S. R. Elliott, J. Engel, *Review of Modern Physics* **80**, 481 (2008)
5. K. Zuber, *Journal of Physics G: Nuclear and Particle Physics* **39**, 124009 (2012)
6. A. S. Barabash, *Physical Review C* **81**, 035501 (2010)
7. J. Schechter, J. W. F. Valle, *Physical Review D* **25**, 11, 2951 (1982)
8. E. Takasugi, *Physics Letters B* **149**, 372 (1984)
9. V. M. Gehman, S. R. Elliott, *Journal of Physics G: Nuclear and Particle Physics* **34**, 4, 667 (2007)
10. J. Engel, G. Hagen, *Physical Review C* **79**, 6, 064317 (2009)
11. J. Barea, F. Iachello, *Physical Review C* **79**, 4, 044301 (2009)
12. T. R. Rodríguez, G. Martínez-Pinedo, *Physical Review Letters* **105**, 252503 (2010)
13. P. K. Rath, R. Chandra, P. K. Raina, et al., *Physical Review C* **85**, 014308 (2012)
14. R. Chandra, K. Chaturvedi, P. K. Rath, et al., *Europhysics Letters* **86**, 3, 32001 (2009)
15. J. Menéndez, D. Gazit, A. Schwenk, *Phys. Rev. Lett.* **107**, 062501 (2011)
16. F. Šimkovic, L. Pacearescu, A. Faessler, *Nuclear Physics A* **733**, 321 (2004)
17. J. H. Thies, T. Adachi, M. Dozono, et al., *Phys. Rev. C* **86**, 044309 (2012)
18. J. H. Thies, D. Frekers, T. Adachi, et al., *Phys. Rev. C* **86**, 014304 (2012)
19. H. Ejiri, *Journal of the Physical Society of Japan* **78**, 7, 074201 (2009)
20. H. Ejiri, *Journal of the Physical Society of Japan* **81**, 3, 033201 (2012)

21. D. Frekers, I. Tanihata, J. Dilling, *Canadian Journal of Physics* **85**, 57 (2007)
22. A. García, Y.-D. Chan, M. T. F. da Cruz, et al., *Physical Review C* **47**, 6, 2910 (1993)
23. S. K. L. Sjøe, D. Melconian, A. García, et al., *Physical Review C* **78**, 6, 064317 (2008)
24. G. Savard, S. Becker, G. Bollen, et al., *Physics Letters A* **158**, 5, 247 (1991)
25. K. Blaum, J. Dilling, W. Nörtershäuser, *Physica Scripta* **2013**, 014017 (2013)
26. J. Dilling, P. Bricault, M. Smith, et al., *Nuclear Instruments and Methods in Physics Research Section B* **204**, 0, 492 (2003)
27. J. Dilling, R. Baartman, P. Bricault, et al., *International Journal of Mass Spectrometry* **251**, 198 (2006)
28. M. Smith, L. Blomeley, P. Delheij, et al., *Hyperfine Interactions* **173**, 0304 (2006)
29. T. Brunner, M. Smith, M. Brodeur, et al., *Nuclear Instruments and Methods in Physics Research Section A* **676**, 0, 32 (2012)
30. G. Sikler, J. C. López-Urrutia, J. Dilling, et al., *The European Physical Journal A - Hadrons and Nuclei* **25**, 63 (2005)
31. A. Lapierre, M. Brodeur, T. Brunner, et al., *Nuclear Instruments and Methods In Physics Research Section A* **624**, 1, 54 (2010)
32. M. Brodeur, V. Ryjkov, T. Brunner, et al., *International Journal of Mass Spectrometry* **310**, 0, 20 (2012)
33. T. Brunner, M. Brodeur, S. Ettenauer, et al., *Journal of Physics: Conference Series* **312**, 072006 (2011)
34. M. Dombisky, P. Bricault, T. Hodges, et al., *Nuclear Physics A* **701**, 486 (2002)
35. P. Kunz, *ISAC-I yield measurements - ISAC e-log entry July 21, 2009 at 1:10am* (2009)
36. T. Brunner, M. Brodeur, C. Champagne, et al., *Nuclear Instruments and Methods In Physics Research Section B* **266**, 19-20, 4643 (2008)
37. J. Katakura, Z. Wu, *Nuclear Data Sheets* **109**, 7, 1655 (2008)
38. K. Krane, *Introductory Nuclear Physics* (Wiley, 1987)
39. T. Brunner, *In-Trap Decay Spectroscopy for $\beta\beta$ Decays*, Ph.D. thesis, Technische Universität München, Munich, Germany (2011)
40. G. F. Knoll, *Radiation Detection and Measurement* (Wiley, 2000)
41. National Nuclear Data Center, *LOGFT version 7.2* (2001)
42. E. Schönfeld, H. Janßen, *Nuclear Instruments and Methods In Physics Research Section A* **369**, 2-3, 527 (1996)
43. A. C. Thompson, D. T. Attwood, E. M. Gullikson, et al., *The X-Ray Data Booklet* (2009), URL <http://xdb.lbl.gov/>
44. Y. Khazov, A. Rodionov, F. Kondev, *Nuclear Data Sheets* **112**, 4, 855 (2011)
45. J. Katakura, K. Kitao, *Nuclear Data Sheets* **97**, 34, 765 (2002)
46. D. A. Dahl, *Int. J. Mass Spectrom.* **200**, 1-3, 3 (2000)
47. T. Brunner, M. Brodeur, P. Delheij, et al., *Hyperfine Interactions* **199**, 191 (2011)
48. A. Lennarz, A. Grossheim, F. Jang, et al., *Hyperfine Interactions* **submitted** (2012)
49. S. Ettenauer, T. Brunner, M. Brodeur, et al., *AIP Conference Proceedings* **1182**, 1, 100 (2009)